Experimental Validation of Driving Force for a Temperature-Sensitive Magnetic Fluid Heat Transport System Utilizing an Electromagnet

Masataka Anazawa*, Keisuke Kusaka
Dept. of Electrical, Electronics, and Information Engineering, Nagaoka University of Technology, Niigata, Japan
*s233091@stn.nagaokaut.ac.jp, kusaka@vos.nagaokaut.ac.jp

***Abstract*— The reliability of high-power-density power converters is a growing concern. Thermal cycling, a major cause of semiconductor failure, necessitates advanced thermal management. Conventional mechanical cooling systems may reduce system lifetime due to mechanical wear. A mechanical-free Temperature-Sensitive Magnetic Fluid (TSMF) cooling system offers a highly reliable alternative. TSMF utilizes temperature-dependent magnetic properties to autonomously transport heat. However, its fundamental characteristics—specifically the driving force and actual cooling capability under an external magnetic field, have not been sufficiently clarified. In this study, an electromagnet-based measurement system was developed to quantitatively evaluate these characteristics for practical TSMF system design. Experimental results revealed that the driving force increases monotonically with increasing magnetic flux density. Furthermore, the system exhibited a load-responsive cooling characteristic, in which the thermal resistance was actively modulated from approximately 11 K/W to 4.5 K/W.**

Keywords—Magnetic fluid, Heat transfer, Passive drive, Power devices cooling.

I. INTRODUCTION

Power converters are widely used in industrial equipment for efficient electrical energy conversion. The reliability of these power converters is a key concern [1–3], especially in industrial applications requiring long-term operation, such as photovoltaic systems [4] and electric vehicles (EVs) [5]. In recent years, there has been a shift in the semiconductor devices used in power conversion circuits from traditional Silicon (Si) semiconductors to wide-bandgap (WBG) semiconductors like SiC and GaN, to achieve higher efficiency.

As mentioned, WBG semiconductors exhibit lower losses and can operate at higher temperatures than Si semiconductors [6–8]. Conversely, the chip area of WBG semiconductors tends to decrease, leading to increased thermal density due to power losses generated within the device [9]. The lifespan of a semiconductor device is highly dependent on thermal cycling [9–11]. As a result, a cooling apparatus capable of effectively dissipating heat from the semiconductor device is required to improve the lifespan and reliability of the power conversion circuit. Such effective cooling is often realized through forced-air cooling utilizing mechanical components.

However, cooling devices equipped with mechanical components are susceptible to mechanical wear and physical degradation [12]. This wear inevitably leads to unexpected cooling failures, thereby decreasing the overall system reliability. Furthermore, the continuous acoustic noise generated by mechanical cooling is often undesirable. For this reason, for power converters operated over long periods, highly reliable and noise-free thermal management using non-mechanical cooling devices is increasingly required. To fulfill this requirement, phase-change cooling technologies have been widely investigated as promising non-mechanical solutions [13]. Notable examples include vapor chambers [14] and immersion cooling, which dissipates heat by submerging devices in dielectric fluids [15]. While these methods achieve high cooling efficiency and silent operation, they face inherent practical limitations. The thermal performance of phase-change cooling is heavily dependent on gravity, resulting in strict constraints on the installation orientation. Additionally, immersion cooling systems introduce significant challenges regarding installation complexities and maintainability [13]. To resolve these issues, a non-mechanical, orientation-independent thermal transport device utilizing the thermomagnetic properties and magnetic force of a magnetic fluid has been proposed [16–18].

Operating without mechanical components, TSMF cooling systems inherently offer a long lifespan and silent operation. However, methods to quantitatively measure the driving force and cooling performance under an external magnetic field have not yet been established. Consequently, a comprehensive design methodology for thermal management systems utilizing TSMF remains unrealized.

This paper proposes the application of a magnetic fluid heat transport system for power device cooling. To characterize the TSMF and collect data for designing the heat transport system, a measurement apparatus utilizing a variable flux electromagnet was developed. Through experimental validation, this study revealed that an increase in the applied magnetic field enhances the driving force, leading to a monotonic decrease in thermal resistance. These findings demonstrate the feasibility of implementing an active thermal management system for cooling power semiconductors.

II. TSMF DRIVING PRINCIPLE

A. Temperature-Sensitive Magnetic Fluid (TSMF)

This study employs a temperature-sensitive magnetic fluid (TSMF) as the working medium. A magnetic fluid consists of nanoscale magnetic particles stably dispersed in a base fluid, possessing both hydrodynamic and magnetic properties. While possessing the fundamental properties of conventional magnetic fluids, TSMF is characterized by a significant decrease in magnetization as the temperature rises near room temperature [16–18]. The fluid utilized in this study is TC3030S (Ferrotec Co.), and its primary physical properties

are summarized in Table 1. Fig. 1 displays the normalized magnetization (M/M_s) of the TSMF as a function of temperature, using 25°C as the baseline. The graph clearly demonstrates that an increase in temperature leads to a reduction in magnetization. Consequently, when the TSMF is heated within an external magnetic field, it experiences a correspondingly weaker magnetic attractive force.

B. *Driving principle*

Fig. 2 shows the operating principle for the TSMF heat transportation system. Heating and cooling regions are established within the TSMF-filled flow path. An electromagnet is positioned across the flow path to apply a magnetic field to the temperature boundary region. With this arrangement, the TSMF is drawn toward the magnetic field application region from both sides of the temperature boundary. This force is called magnetic volume force $\boldsymbol{F_m}$ [N/m^3] [16–18]. The magnitude of the magnetic volume force depends on the product between the magnetization $\boldsymbol{M}$ [A/m] and the magnetic field gradient $\boldsymbol{H}$ [A/m].

$$\boldsymbol{F_m} = \mu_0(\boldsymbol{M}\cdot\nabla\boldsymbol{H}) \tag{1}$$

In the TSMF flow path, the reduction of magnetization as temperature rises on the high-temperature side induces a magnetic imbalance between the cold and hot regions. This thermally induced shift in magnetization further creates a non-uniform state in the magnetic volume force. As a result, a pressure difference $\Delta\boldsymbol{P}$ [Pa] is generated in the direction from the low-temperature region to the high-temperature region. When the system is configured in a closed loop, this driving force acts as a circulating force, enabling the TSMF to effectively transport heat without any mechanical driving parts.

$$\Delta\boldsymbol{P} = \boldsymbol{F_{Tlow}} - \boldsymbol{F_{Thigh}} \tag{2}$$

III. Driving Force Measurement

A driving force is generated by the temperature difference and the applied external magnetic field in the magnetic fluid. To quantitatively assess this phenomenon, a driving force measurement device using an electromagnet was developed. Under various magnetic field strengths and temperature differences, the apparatus clarifies the fundamental driving characteristics of the TSMF.

A. *Driving Force Measuring Instrument*

To systematically control the external magnetic field, a custom C-shaped electromagnet was developed using assembled electromagnetic steel sheets (35H440, Nippon Steel Co.). The core features an 8 mm gap and a 30 mm width along the flow path to concentrate the magnetic field at the temperature boundary. The applied DC magnetic flux density was estimated by fitting a curve to the pre-measured relationship under 50 Hz AC excitation. Specifically, the electromagnet generates approximately 0.41 T at a DC current of 4.0 A. A stabilized DC power supply was used to provide a constant excitation current to the electromagnet, ensuring a stable magnetic field.

While the fundamental structure of the driving-force measurement apparatus is based on our previous work [19], the current setup introduces precise magnetic-field control via an electromagnet and an active temperature-difference control mechanism. A measurement device capable of evaluating the driving force of TSMF as pressure was developed. Fig. 3

Table 1. Physical properties of TC3030S.

Properties	Symbol	Value
Dispersion medium		Synthetic hydrocarbons
Saturation magnetic flux density @25°C	B_{sat}	30.0 mT
Density @25°C	ρ	1.17×10^3 kg/m^3
Thermal conductivity @22°C	λ	0.143W/(m·K)
Specific heat	C_p	1420 J/(kg·K)

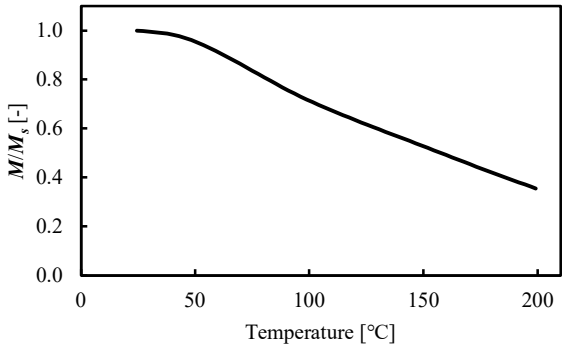

Fig. 1. Normalized magnetization versus temperature for TC3030S.

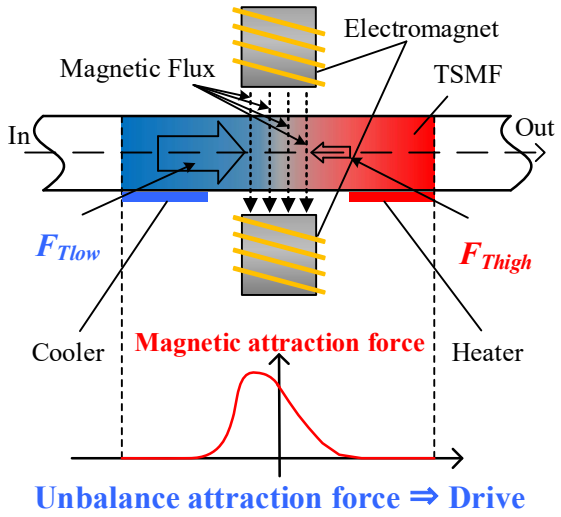

Fig. 2. Magnetic fluid driving principle.

shows a schematic diagram of the measuring instrument. Measurement of the liquid column height enables evaluation of the driving force produced in the TSMF. T The device is arranged as a U-shaped tube filled with TSMF and leveled parallel to the ground, ensuring that both liquid column heights are identical in the initial state. By creating a temperature difference across the magnetic field application region, a driving force is generated from the cooling side toward the heating side.

Consequently, the liquid column on the heating side rises while the cooling side descends. By measuring the difference in liquid column heights, the driving force within the TSMF can be quantitatively evaluated.

The driving pressure difference $\Delta\boldsymbol{P}$ [Pa] generated by the magnetic volume force is calculated based on three parameters: the fluid density ρ [kg/m^3], the gravitational

acceleration $\boldsymbol{g}$ [m/s^2], and difference in liquid column height Δh [m] [20]. Here, the influence of thermal expansion is experimentally compensated to isolate the magnetic response. The driving force $\boldsymbol{F}$ [N] is obtained by multiplying $\Delta \boldsymbol{P}$ by the cross-sectional area A [m^2] of the tube.

$$\boldsymbol{F} = \Delta \boldsymbol{P} \cdot A = \rho \boldsymbol{g} \Delta h A \quad (3)$$

Fig. 4 shows the experimental setup used for measuring the driving force of the TSMF. As shown in Figs. 3 and 4, the experimental apparatus comprises a U-shaped tube constructed from copper and glass tubing, a central magnetic field supply unit, heating and cooling modules on opposite sides, a liquid level measurement section, and thermocouples for thermal monitoring.

The U-shaped configuration is constructed by connecting a copper pipe (7 mm inner diameter) and a glass tube (6 mm inner diameter) using tube fittings. Additionally, the central 40 mm section of the copper pipe has a flattened internal cross-section measuring 7 mm in width and 1 mm in height. The cooling section consists of an aluminum plate through which temperature-controlled cooling water from a chiller circulates, clamping the copper pipe from both sides. The heating section is constructed by winding a spiral heater around the copper pipe. During the measurement, the power supplied to the spiral heater is controlled based on the temperature readings from these thermocouples to maintain a constant temperature difference at the magnetic field application region. The liquid column height is measured using graduated scales attached to both the left and right glass tubes.

B. Driving Force Characteristics

As described previously, the mechanism that drives TSMF depends on both the applied magnetic field and the temperature gradient. For a precise evaluation of how the magnetic field alone affects this force, the temperature difference must be kept uniform throughout the measurement.

In this experiment, the temperature of the cooling water supplied to the cooling plate was fixed at 20°C, and temperature differences of 2°C, 6°C, and 10°C were applied across the electromagnet. The influence of thermal expansion of the TSMF liquid was minimized in the measurements. Under these conditions, the magnetic flux density produced by the electromagnet was gradually increased in steps of approximately 0.1 T. The corresponding driving force response is shown in Fig. 5.

All measurements were conducted under steady-state conditions. After setting the temperature difference, the system was allowed to stabilize for 30 min before measurements were taken. In addition, after each change in the applied magnetic field, a 15min stabilization period was observed before recording the driving force. During the steady-state measurement intervals, the temperature difference was maintained within ±0.5°C of the target value.

To reduce the influence of thermal expansion, the liquid column height was first confirmed under the applied temperature difference without applying the magnetic field. The magnetic field was then gradually applied from this reference condition to measure the driving force.

From the experimental results, the driving force increases with increasing temperature difference regardless of the applied magnetic field. This tendency is consistent with the

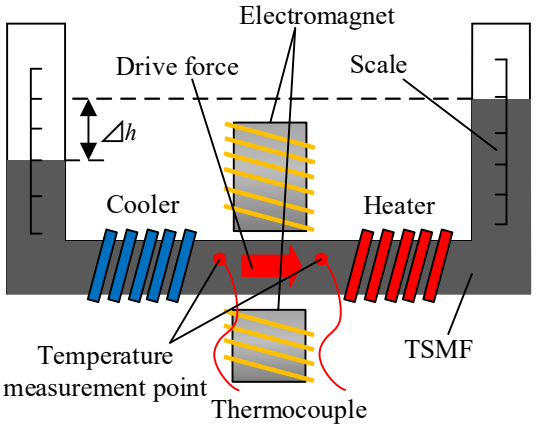

Fig. 3 Schematic diagram of the driving force measurement apparatus.

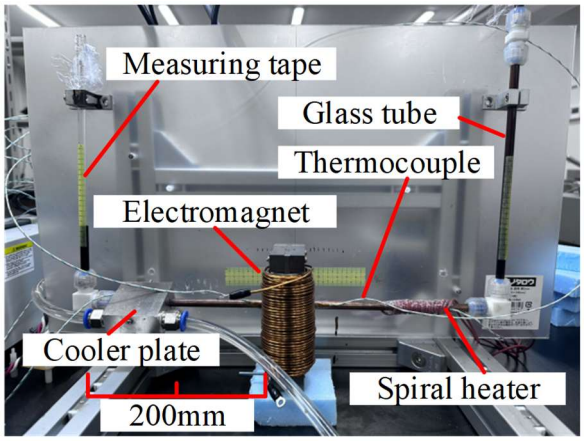

Fig. 4 Drive force measurement instrument setup.

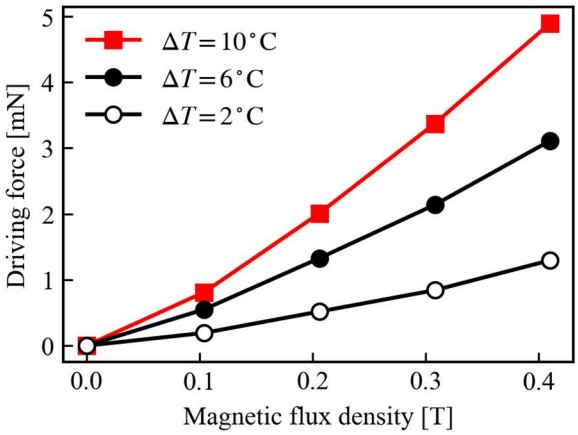

Fig. 5 Driving force characteristics.

results reported in our previous study [19]. Furthermore, for each temperature difference, the driving force increases monotonically with increasing magnetic flux density. This phenomenon likely stems from the intensification of the magnetic field gradient as magnetic flux density rises. These results demonstrate that the driving force of TSMF strongly depends on the applied magnetic field.

In contrast, this dependence exhibits a quadratic-like trend rather than the theoretical linear increase expected for the TSMF, which magnetically saturates at approximately 30

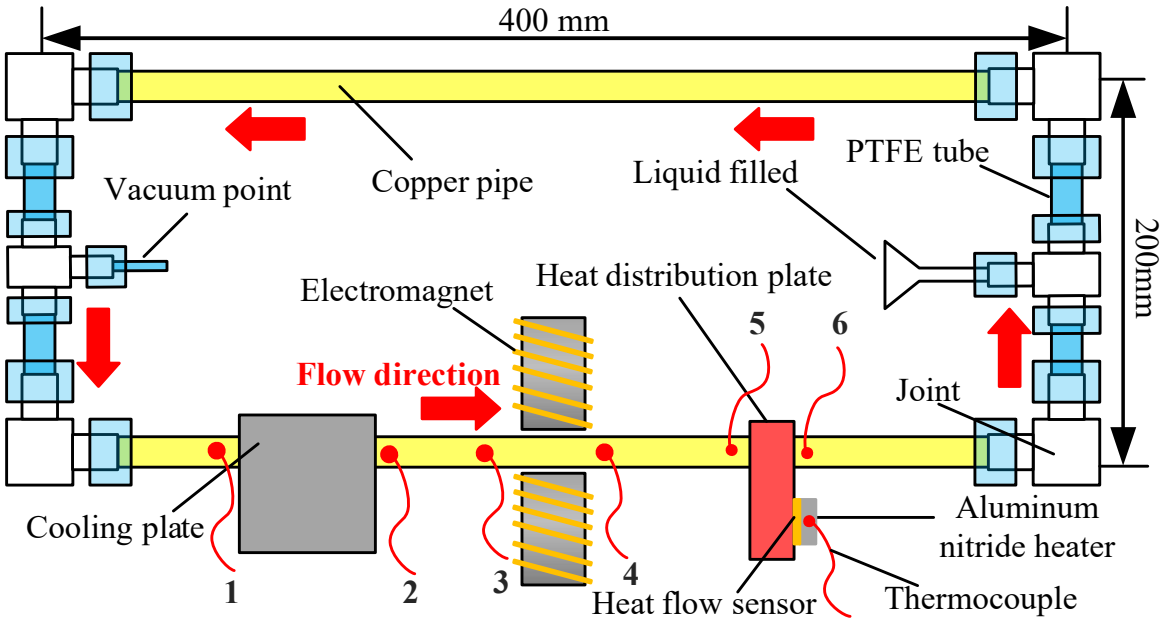

Fig. 6 Schematic diagram of the heat transport measurement apparatus.

mT. This discrepancy may be attributed to factors such as magnetic circuit nonlinearity and fringing magnetic flux in the gap region. As the external magnetic field intensity rises, the fringing magnetic flux proliferates, extending the magnetic influence into the adjacent space. This results in an increase in the volume of magnetized TSMF within the region experiencing the temperature difference. Consequently, this increase in the amount of magnetized fluid non-linearly enhances the integrated driving force. This interpretation is consistent with the expansion of the effective magnetic field region.

IV. HEAT TRANSPORT

In the previous section, it was confirmed that the driving force in TSMF depends on both the applied magnetic field and the temperature difference. In this section, the heat transport performance of a closed-loop TSMF system utilizing this driving force is experimentally evaluated.

A. Heat Transport Measuring Instrument

The heat transport measurement apparatus is an improved version of our previous device, featuring a heat flux sensor for accurate heat input measurement and an electromagnet for external magnetic field supply. In the present setup, the magnetic field supply unit was replaced with an electromagnet in order to control the applied magnetic field. As shown in Fig. 6, the apparatus comprises a closed-loop channel containing TSMF, along with a heating section, a cooling section, and an electromagnet. The total length of this flow path is approximately 1.2 m.

In the heating section, an aluminum nitride (AlN) heater (Sakaguchi Electric Heater, WALN-6, 12 mm × 12 mm) was used to simulate the heat load generated by semiconductor devices. The heater was sandwiched between brass heat equalization plates to ensure temperature uniformity. The electrical power supplied to the heater was controlled using a DC stabilized power supply so that a constant heat input was applied to the system. To monitor the thermal input into the heat transport system, a heat flux sensor (DENSO D0004TC) was positioned between the heater and the pipe. Based on the findings of our previous study, the heating and cooling sections were positioned approximately 20 mm from the electromagnet.

The cooling section employs the same structure as the driving force measurement apparatus, where cooling water circulates through aluminum plates that clamp the copper pipe. The flow path consists of two types of conduits: copper pipes (7 mm inner diameter) and PTFE tubes (6 mm inner diameter). The loop was vacuum-filled with TSMF to eliminate air bubbles and ensure complete filling of the flow path. During the measurements, the entire flow path was covered with glass wool to suppress heat loss to the surrounding air. In addition, thermal insulation (Styrofoam manufactured by DuPont Styro Co.) was placed between the apparatus and the desk to further reduce heat loss to the desk. Thermocouples were installed at several locations along the flow path to monitor the temperature distribution in the loop.

B. Measuring methods

In this study, the thermal resistance is used as an index to evaluate the heat transport capability of the TSMF system. The thermal resistance R_{th} [K/W] is calculated as the temperature difference between the heating section and the cooling section divided by the supplied heat input [21].

Heating and cooling section temperatures were acquired via thermocouples installed at the inlet and outlet of the heat equalization plate (TC5 and TC6) and the cooling plate (TC1 and TC2), respectively. The average temperatures of these thermocouples were defined as the heating-side temperature T_h and the cooling-side temperature T_c and the supplied heat input is denoted as Q.

$$R_{th} = \frac{T_h - T_c}{Q} \tag{4}$$

The supplied heat input Q [W] was determined from the heat flux measured by the heat flux sensor installed in the heating section. The measured heat flux is denoted as q [W/m^2], and the heater surface area of the AlN heater is denoted as A_h [m^2].

$$Q = qA_h \tag{5}$$

Although the sensing area of the heat flux sensor is slightly smaller than the heater area, thermal interface sheets were used to cover the heater surface so that the heat flux was uniformly transferred to the sensor. Furthermore, the entire measurement apparatus was thermally insulated to minimize heat loss to the surroundings. Also, to the thermal resistance, the flow velocity of the TSMF was estimated. Because the TSMF used in this study is black and slightly viscous, direct visual observation of the flow is difficult. Thus, the flow velocity $\boldsymbol{U}$ [m/s] was estimated using a calorimetric method based on the temperature rise across the heating section. The density of the fluid is denoted as ρ [kg/m^3], the specific heat as c_p [J/(kg·K)], the cross-sectional area of the flow path as A [m^2], and the temperature difference across the heating section ΔT [°C] was calculated from the temperatures measured by thermocouples TC6 and TC5.

$$\Delta T = T_{TC6} - T_{TC5} \tag{6}$$

$$\boldsymbol{U} = \frac{Q}{\rho \cdot c_p \cdot A \cdot \Delta T} \tag{7}$$

C. *Operation test of the heat transport system*

To confirm the operation of the proposed TSMF heat transport system, a time-dependent experiment was conducted with a heater input power of 5 W. During the experiment, the temperature of the cooling water supplied to the cooling plate was maintained at 20°C.

Fig. 8 shows the variation of the heater temperature when a magnetic field is applied. First, the system was operated without applying a magnetic field until the heater temperature reached a steady state. After approximately 90 min., a magnetic field corresponding to a magnetic flux density of 0.31 T was applied using the electromagnet. As a result, the heater temperature decreased from 91.7°C to 64.9°C, a reduction of 26.8°C. This temperature reduction suggests that the application of the magnetic field initiates circulation of the TSMF in the closed loop, thereby enhancing heat transport from the heating section to the cooling section. Since the heater input power and cooling conditions were held constant during the experiment, the observed temperature reduction is primarily attributed to heat transport induced by the applied magnetic field.

D. *Heat transport performance*

The heat transport performance of the proposed TSMF system was evaluated using the thermal resistance defined in the previous section. Fig. 9 shows the relationship between thermal resistance and magnetic flux density under different heater input power conditions (2.5 W, 5.0 W, and 7.5 W). For all heater input power conditions, the thermal resistance decreases as the magnetic flux density increases. This tendency indicates that the heat transport capability of the system improves with increasing applied magnetic field. The improvement is attributed to the increase in the driving force of the TSMF, which enhances the fluid circulation and promotes heat transport.

However, the reduction in thermal resistance becomes less significant above approximately 0.2 T. This observation suggests that the heat transport performance is closely related to the flow velocity of the TSMF. The total thermal resistance in the system is governed by both the sensible heat transport

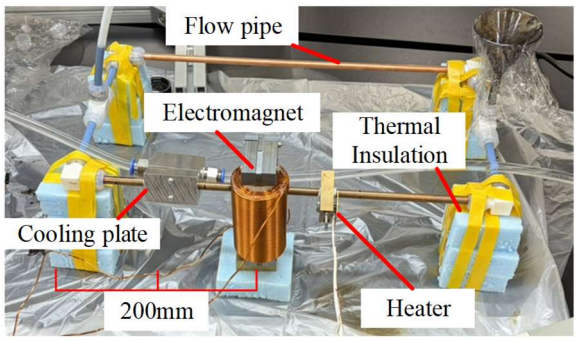

Fig. 7 Heat transport measurement instrument setup (Glass wool not installed).

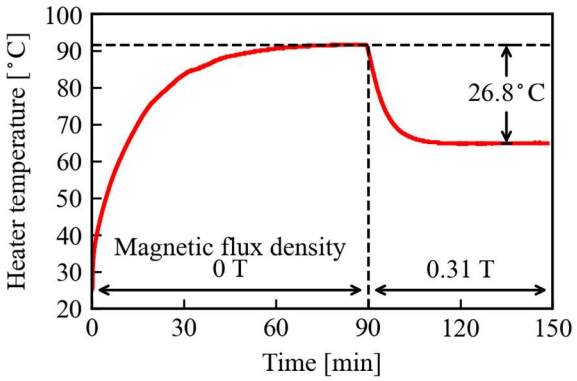

Fig. 8 Operation test.

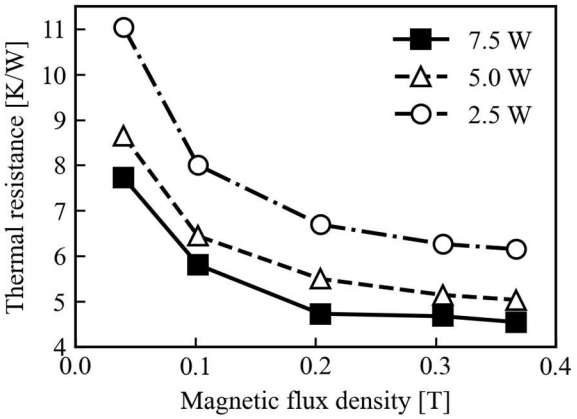

Fig. 9 Thermal resistance as a function of magnetic flux density for different heater input powers.

and the convective heat transfer at the boundary. Since the convective thermal resistance scales with the flow velocity to a fractional power rather than a strict inverse proportion, the overall thermal resistance decreases with velocity, but its rate of decrease diminishes at higher flow velocities [22]. Accordingly, the relationship between flow velocity and thermal resistance is shown in Fig. 10.

As shown in Fig. 10, although some variations exist with heater input power, the overall trend indicates that the thermal resistance decreases with increasing flow velocity, with a diminishing rate of decrease at higher velocities. This result is consistent with the general characteristics of convective heat transfer.

Another important feature observed in Fig. 9 is the dependence of thermal resistance on heater input power. For all magnetic field conditions, the thermal resistance decreases

as the heater input power increases. This result indicates that the heat transport performance of the TSMF system improves under larger heat loads. In the present system, the thermal resistance varies from approximately 11 K/W to 4.5 K/W depending on the applied magnetic field and heater input power. This result suggests that the thermal resistance of the TSMF system can be adjusted by controlling both the applied magnetic field and the heat load. Also, under the maximum heater input condition of 7.5 W, a transported heat load of approximately 5.8 W was measured by the heat flux sensor.

This behavior can be explained by the driving force characteristics of the TSMF. As confirmed in the previous section, the driving force of the TSMF depends on both the temperature difference and the applied magnetic field. An increase in heat load widens the temperature difference in the magnetic field region, thereby increasing the driving force of the TSMF. Also, increasing the magnetic field strength further enhances the driving force, resulting in improved heat transport performance.

CONCLUSION

In this study, an electromagnet-based measurement apparatus was developed to clarify the fundamental driving characteristics and cooling performance of a TSMF cooling system. Experimental results demonstrated that both the driving force and the cooling performance depend on the applied magnetic field and the temperature difference. Specifically, the thermal resistance exhibited a monotonic decrease from approximately 11 K/W to 4.5 K/W as flow velocity increased. Furthermore, the proposed system achieved a maximum heat transport capacity of 5.8 W, demonstrating load-responsive cooling, in which the thermal resistance decreases as the heat load increases.

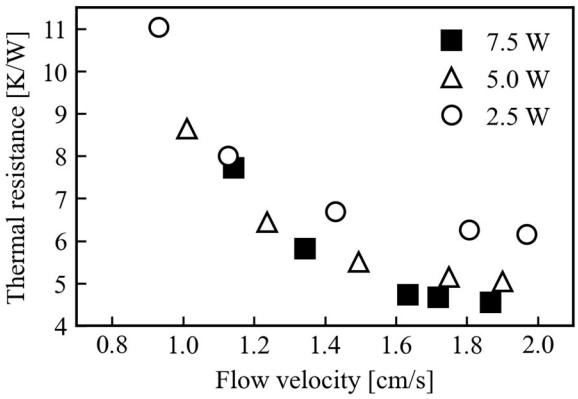

Fig. 10 Thermal resistance as a function of flow velocity.

REFERENCES

[1] M. Andresen, J. Kuprat, V. Raveendran, J. Falck and M. Liserre, "Active thermal control for delaying maintenance of power electronics converters," in Chinese Journal of Electrical Engineering, vol. 4, no. 3, pp. 13-20, September 2018.

[2] Y. Song and B. Wang, "Survey on Reliability of Power Electronic Systems," in IEEE Transactions on Power Electronics, vol. 28, no. 1, pp. 591-604, Jan. 2013.

[3] H. Wang, M. Liserre and F. Blaabjerg, "Toward Reliable Power Electronics: Challenges, Design Tools, and Opportunities," in IEEE Industrial Electronics Magazine, vol. 7, no. 2, pp. 17-26, June 2013.

[4] Q. Mu, J. Zhou, L. Wang and T. Zhao, "Universal Reliability Assessment of Inverters in Photovoltaic Systems Based on Real-Field Mission Profiles," 2024 IEEE Energy Conversion Congress and Exposition (ECCE), Phoenix, AZ, USA, 2024, pp. 4246-4252.

[5] F. Blaabjerg, H. Wang, I. Vernica, B. Liu and P. Davari, "Reliability of Power Electronic Systems for EV/HEV Applications," in Proceedings of the IEEE, vol. 109, no. 6, pp. 1060-1076, June 2021.

[6] X. She, A. Q. Huang, Ó. Lucía and B. Ozpineci, "Review of Silicon Carbide Power Devices and Their Applications," in IEEE Transactions on Industrial Electronics, vol. 64, no. 10, pp. 8193-8205, Oct. 2017.

[7] A. E. Islam, N. P. Sepelak, A. T. Miesle, H. Lee, M. Snure, and S. Nikodemski, et al., "Effect of High Temperature on the Performance of AlGaN/GaN T-Gate High-Electron Mobility Transistors With ~140-nm Gate Length," IEEE Transactions on Electron Devices, vol. 71, Issue 3, 2024.

[8] J. Millán, "A review of WBG power semiconductor devices," CAS 2012 (International Semiconductor Conference), Sinaia, Romania, pp. 57-66, 2012.

[9] E. Agirrezabala, I. Aizpuru, D. Garrido and A. Portillo, "Reliability of Power Semiconductor Modules: A State-of-the-Art Review," in IEEE Open Journal of Power Electronics, vol. 6, pp. 1036-1067, 2025.

[10] S. Fukunaga, Y. Nakamura, and T. Funaki, "Evaluation of Electrical Model Parameter Changes in SiC Power MOSFETs During Power Cycling Test," IEEJ Journal of Industry Applications, vol. 13, Issue 6, pp. 731–740, 2024.

[11] J. Zhang, H. Shen, H.Sun and Z. Wang, "Review on the Thermal Models Applications in the Reliability of Power Semiconductor Device," IET Power Electronics, vol. 18, Issue 1, 2025.

[12] M. Polikarpova, M. Lohtander, L. Popova, T. Musikka, R. Juntunen and J. Pyrhönen, et al., "Reliability analysis of liquid cooling systems' mechanical components for 3 MVA power converter," ISSN 1392-1207, Mechanika, vol. 19, no. 14, 2013.

[13] S. M. I. Rahman, A. Moghassemi, A. Arsalan, L. Timilsina, P. K. Chamarthi and Behnaz Papari, et al., "Emerging Trends and Challenges in Thermal Management of Power Electronic Converters: A State of the Art Review," in IEEE Access, vol. 12, pp. 50633-50672, 2024.

[14] W. Mu, L. Wang, H. Jin, B. Hu, B. Wang and Teng Long. et al., "Near Junction Integration of Vapor Chamber for Transient Thermal Performance Improvements of SiC Power Module," in IEEE Open Journal of Power Electronics, vol. 6, pp. 286-299, 2025.

[15] A. Ristic-Smith and D. J. Rogers, "Compact Two-Phase Immersion Cooling With Dielectric Fluid for PCB-Based Power Electronics," in IEEE Open Journal of Power Electronics, vol. 5, pp. 1107-1118, 2024.

[16] Z. Rong, Y. Iwamoto, Y. Ido, A. Mitani, and R. Kobayashi, "Investigation of heat transfer characteristics of the self driving temperature-sensitive magnetic fluid through a nonmagnetic porous in a heating pipe, " Journal of Magnetism and Magnetic Materials, vol. 590, article id. 171658, 2024.

[17] K. Fujimoto, M. Ikegawa, and H. Yamagishi, "Study on Mini-Heat Transfer Device Using Temperature-Sensitive Magnetic Fluid", Transactions of the Japan Society of Mechanical Engineers, Series B. , vol. 72, No. 723, pp. 179–185, 2006.

[18] W. Xin-hua, J. Yu-lin, N. Yong-chao and Y. Jie, "Study on Enhanced Heat Transfer Features of Nano-magnetic Fluid Heat Pipe Under Magnetic Field," International Journal of Heat and Technology, vol.33, No.1, pp. 137–144, 2015.

[19] M. Anazawa, M. Suzuki, M. Baba and K. Kusaka, "Self-Driven Magnetic Fluid Cooling for Power Devices Utilizing Permanent Magnet," 2025 14th International Conference on Renewable Energy Research and Applications (ICRERA), Vienna, Austria, 2025, pp. 1002-1007.

[20] Japan Society of Mechanical Engineers, JSME Textbook Series Fluid Mechanics, pp. 29, 2018.

[21] E. Sadeghinezhad, A. R. Akhiani, H. S. C. Metselaar, S. T. Latibari, M. Mehrali, and M. Mehrali, "Parametric study on the thermal performance enhancement of a thermosyphon heat pipe using covalent functionalized graphene nanofluids," Applied Thermal Engineering, vol. 175, 2020, Art. No. 115385.

[22] T. L. Bergman, A. S. Lavine, F. P. Incropera, and D. P. DeWitt, "Fundamentals of Heat and Mass Transfer," 7th ed. Hoboken, NJ: John Wiley & Sons, 2011.